Central-spindle microtubules are strongly coupled to chromosomes during both anaphase A and anaphase B

Che-Hang Yu[a,b,†,*], Stefanie Redemann[c,d,†], Hai-Yin Wu[e], Robert Kiewisz[c], Tae Yeon Yoo[f], William Conway[e], Reza Farhadifar[a,f,g], Thomas Müller-Reichert[c,‡], and Daniel Needleman[a,f,‡]

[a]John A. Paulson School of Engineering and Applied Sciences, [e]Department of Physics, and [f]Department of Molecular and Cellular Biology, Harvard University, Cambridge, MA 02138; [b]Electrical and Computer Engineering, University of California, Santa Barbara, Santa Barbara, CA 93106; [c]Experimental Center, Faculty of Medicine Carl Gustav Carus, Technische Universität Dresden, 01307 Dresden, Germany; [d]Center for Membrane and Cell Physiology & Department of Molecular Physiology and Biological Physics, University of Virginia, Charlottesville, VA 22903; [g]Center for Computational Biology, Flatiron Institute, Simons Foundation, New York, NY 10010

ABSTRACT **Spindle microtubules, whose dynamics vary over time and at different locations, cooperatively drive chromosome segregation. Measurements of microtubule dynamics and spindle ultrastructure can provide insight into the behaviors of microtubules, helping elucidate the mechanism of chromosome segregation. Much work has focused on the dynamics and organization of kinetochore microtubules, that is, on the region between chromosomes and poles. In comparison, microtubules in the central-spindle region, between segregating chromosomes, have been less thoroughly characterized. Here, we report measurements of the movement of central-spindle microtubules during chromosome segregation in human mitotic spindles and *Caenorhabditis elegans* mitotic and female meiotic spindles. We found that these central-spindle microtubules slide apart at the same speed as chromosomes, even as chromosomes move toward spindle poles. In these systems, damaging central-spindle microtubules by laser ablation caused an immediate and complete cessation of chromosome motion, suggesting a strong coupling between central-spindle microtubules and chromosomes. Electron tomographic reconstruction revealed that the analyzed anaphase spindles all contain microtubules with both ends between segregating chromosomes. Our results provide new dynamical, functional, and ultrastructural characterizations of central-spindle microtubules during chromosome segregation in diverse spindles and suggest that central-spindle microtubules and chromosomes are strongly coupled in anaphase.**

Monitoring Editor
Yixian Zheng
Carnegie Institution

Received: Jan 31, 2019
Revised: Jul 8, 2019
Accepted: Jul 19, 2019

INTRODUCTION

Chromosome segregation is the essential biological processes in which chromosomes are partitioned into the two daughter cells during cell division. In eukaryotes, chromosome segregation is carried out by the spindle, which is predominately composed of microtubules. Chromosomes first align in the middle of the spindle and are then segregated in anaphase. It is often the case that chromosome segregation is accompanied by an elongation of the spindle. In many systems, the speed of spindle elongation is slower

This article was published online ahead of print in MBoC in Press (http://www.molbiolcell.org/cgi/doi/10.1091/mbc.E19-01-0074) on July 24, 2019.

The authors declare no competing financial interests.

[†]These authors contributed equally to this work.

[‡]These authors co-advised this work.

Author contributions: C.-H.Y. and D.N. conceived and designed the research; C.-H.Y. and W.C. performed optical measurements and quantitative analysis; S.R., R.K., and T.M.R. performed electron tomography and 3D reconstructions; H.Y.W. and C.H.-Y. built the home-made laser ablation system; C.H.-Y., H.Y.W., and R.F. prepared *C. elegans* samples; T.Y.Y. and C.-H.Y. cloned and prepared human tissue culture cells; the manuscript was written by C.-H.Y. and D.N. and commented by S.R. and T.M.R.

*Address correspondence to: Che-Hang Yu (chehangyu@gmail.com).

Abbreviation used: RNAi, RNA interference.

than chromosome segregation, such that chromosomes move closer to spindle poles over the course of anaphase. The movement of the chromosomes toward spindle poles is referred to as anaphase A; the elongation of the spindle (i.e., the separation of spindle poles) is referred to as anaphase B. The motion of anaphase A and anaphase B has been thought to depend on different behaviors of microtubules at different parts of the spindle (Scholey *et al.*, 2016; Asbury, 2017).

The movement and turnover of spindle microtubules in anaphase have been measured with a variety of techniques, including photobleaching (Mallavarapu *et al.*, 1999; Khodjakov *et al.*, 2004; Redemann *et al.*, 2017), photoconversion/photoactivation (Mitchison and Salmon, 1992; Ferenz *et al.*, 2010; Vukusic *et al.*, 2017), and fluorescence speckle microscopy (Brust-Mascher *et al.*, 2004; Cameron *et al.*, 2006; Pereira *et al.*, 2016). Many previous studies have focused on characterizing kinetochore microtubule dynamics, providing great insights into the mechanisms of spindle assembly (Mitchison, 1989; Maiato *et al.*, 2005; Cameron *et al.*, 2006; Ma *et al.*, 2010; Redemann *et al.*, 2017) and the poleward chromosome motion in anaphase A and anaphase B (Mitchison and Salmon, 1992; Brust-Mascher *et al.*, 2004; LaFountain *et al.*, 2004). The behaviors of microtubules in the central-spindle, between segregating chromosomes, have been less thoroughly characterized than kinetochore microtubules. It has been shown that microtubules of the central-spindle slide apart while spindles elongate in diatoms, yeasts, flies, and human cells (Saxton and McIntosh, 1987; Masuda *et al.*, 1988; Mallavarapu *et al.*, 1999; Scholey *et al.*, 2016; Vukusic *et al.*, 2017). However, we are aware of few studies that *simultaneously* measure the speeds of central-spindle microtubules and chromosomes (Vukusic *et al.*, 2017) during anaphase A and anaphase B. Such data are potentially interesting, as they might provide further insight into the role of central-spindle microtubules in chromosome segregation. Formally, there are three possibilities: central-spindle microtubules might move slower, faster, or at the same speed as segregating chromosomes (Figure 1).

While simultaneous observation of microtubule and chromosome dynamics can reveal whether their motions are correlated, perturbing spindle microtubules provides a means to test the extent to which their motions are coupled to the motion of chromosomes. A number of groups have used laser ablation to cut selected populations of microtubules and concluded that, in some anaphase spindles, central-spindle microtubules resist pulling forces from astral microtubules (Aist and Berns, 1981; Aist and Bayles, 1991; Aist *et al.*, 1993; Kronebusch and Borisy, 1981; Grill *et al.*, 2001); in some anaphase spindles, central-spindle microtubules exert pushing forces that contribute to anaphase chromosome motion (Khodjakov *et al.*, 2004; Nahaboo *et al.*, 2015; Laband *et al.*, 2017; Vukusic *et al.*, 2017). However, perturbation experiments must always be interpreted with care. One complication is the potential for redundant mechanisms. Thus, the observation that chromosome segregation can proceed without a connection to spindle poles in many systems (Nicklas, 1989; Khodjakov *et al.*, 2004; Elting *et al.*, 2014; Nahaboo *et al.*, 2015; Vukusic *et al.*, 2017) is equally consistent with two different explanations: that a loss of connection to the pole can be compensated by alternative processes, or that pole connections minimally contribute to chromosome motion. Another concern with any perturbation experiment is the possibility of collateral damage/off-target effects. These concerns can be minimized (but not eliminated) by focusing on the immediate response to a rapid perturbation using a technique with a highly localized impact. In this regard, laser ablation with femtosecond pulses is advantageous, as cuts can be performed in seconds with ~300 nm resolution with no discernible impact outside of the ablated region (Konig *et al.*, 1999; Schaffer *et al.*, 2001a,b; Watanabe *et al.*, 2004; Shen *et al.*, 2005; Supatto *et al.*, 2005; Vogel *et al.*, 2005; Chung *et al.*, 2006; Gattass and Mazur, 2008; Vitek *et al.*, 2010), unlike ablation with other lasers which can produce a significant amount of denatured protein (Brenner *et al.*, 1980; Khodjakov *et al.*, 1997, 2000).

Light microscopy has insufficient resolution to resolve individual microtubules in spindles. Thus, a detailed study of spindle architecture requires alternative techniques, such as electron microscopy (Muller-Reichert *et al.*, 2018). The structure of central-spindle microtubules has been studied using electron microscopy in a number of spindles, which has revealed different structures in different spindles. In yeast and diatom spindles, central-spindle microtubules span from the middle of the spindle to the poles (McDonald *et al.*, 1977, 1979; Ding *et al.*, 1993; Winey *et al.*, 1995, 2005). In contrast, in PtK1 mitotic spindles, many central-spindle microtubules have both ends between chromosomes, while other central-spindle microtubules extend from the interchromosomal region and terminate around kinetochore fibers (Mastronarde *et al.*, 1993). In *Caenorhabditis elegans* female meiotic spindles, partial electron microscopy reconstruction revealed that many central-spindle microtubules have both ends between chromosomes, some of which

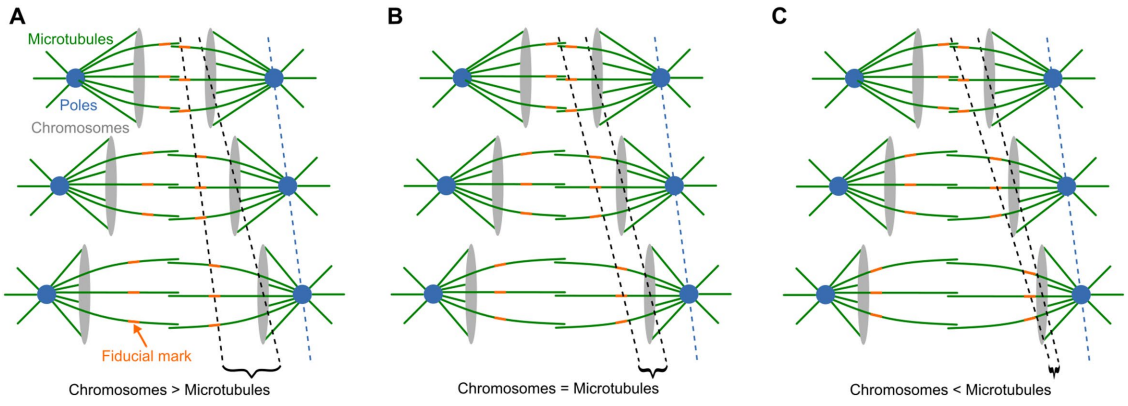

FIGURE 1: Possible relative speeds of central-spindle microtubules and chromosomes when anaphase A and anaphase B occur simultaneously. Central-spindle microtubules might (A) move slower than chromosomes; (B) move at the same speed as chromosomes; (C) move faster than chromosomes. For each case, the motion of a fiducial mark on central-spindle microtubules (orange), chromosomes (gray), and spindle poles (blue) is indicated.

appear to make end-on contacts to chromosomes (Laband *et al.*, 2017; Redemann *et al.*, 2018). These different structures make it unclear to what extent central-spindle microtubules are coupled to chromosomes in different spindles.

In this work, we investigated the relationship between central-spindle microtubules and chromosomes during anaphase in human mitotic spindles and *C. elegans* mitotic and female meiotic spindles. We used the same laser ablation and electron microscopy techniques on all of these spindles to avoid the potential complications of interpretation that can arise when different techniques are applied to different systems. We found that central-microtubules slide apart at the same speed as chromosomes, even when chromosomes move closer to poles. Damaging the central-spindle microtubules by laser ablation caused immediate and complete cessation of chromosome motion, even when anaphase A and anaphase B occur simultaneously, suggesting a strong coupling between central-spindle microtubules and chromosomes. Our electron tomographic reconstructions further reveal that these anaphase spindles all contain microtubules with both ends between segregating sister chromosomes and other central-spindle microtubules that terminate on either chromosomes or kinetochore fibers. Taken together, this work suggests that central-spindle microtubules are strongly coupled to chromosomes in anaphase spindles.

RESULTS

Central-spindle microtubules slide apart at the speed of chromosome motion in anaphase human mitotic spindles

We set out to simultaneously measure the relative motion of central-spindle microtubules and chromosomes by generating a stable human cell line expressing mEOS3.2::tubulin and GFP::CENP-A. This cell line allowed us to photoconvert a subset of labeled microtubules between chromosomes while simultaneously tracking the motion of kinetochores and poles. We focused on studying chromosome motion 30–60 s after the onset of anaphase. Tracking the motions of kinetochores and spindle poles reveals that, at this time, chromosomes move away from the center of the spindle with a speed of 2.7 ± 0.2 μm/min, while poles move away from the spindle center at a speed of 1.5 ± 0.1 μm/min ($n = 8$, $p < 10^{-4}$ compared with chromosome-to-spindle center moving speed), so the chromosome-to-pole distance decreases at a speed of 1.2 ± 0.2 μm/min (Figure 2A). Thus, our experiments probe a time window in which the speed of chromosome-to-pole motion is similar to the speed of pole-to-spindle center motion ($p = 0.19$), that is, anaphase A and anaphase B were both underway at this time. Next, a line of fluorescence-labeled microtubules across the spindle was photoconverted 30–60 s after the onset of anaphase. The single line of photoconverted tubulin split apart over time, demonstrating the sliding of central-spindle microtubules (Figure 2B, magenta; Supplemental Movie S1). The total fluorescence intensity of the photoconverted tubulin was tracked over time and was fitted well by a single exponential with a characteristic decay time of τ = 21 ± 0.3 s. Kymographs revealed that the speed of central-spindle microtubule sliding was similar to the speed of chromosome motion and substantially faster than pole motion (Figure 2C). To quantify the speed of the central-spindle microtubules, we took line profiles and tracked the motion of photoactivated regions (Figure 2D), in addition to chromosomes and poles (see *Materials and Methods*). We found that the photoconverted microtubules slide at a speed of 2.8 ± 0.1 μm/min ($n = 46$), which is indistinguishable from the speed of chromosome motion, 2.7 ± 0.1 μm/min, ($n = 46$, $p = 0.85$) and substantially greater than the speed of pole motion, 1.5 ± 0.1 μm/min ($n = 46$, $p < 10^{-11}$) (Figure 2D, right). This result shows that central-spindle

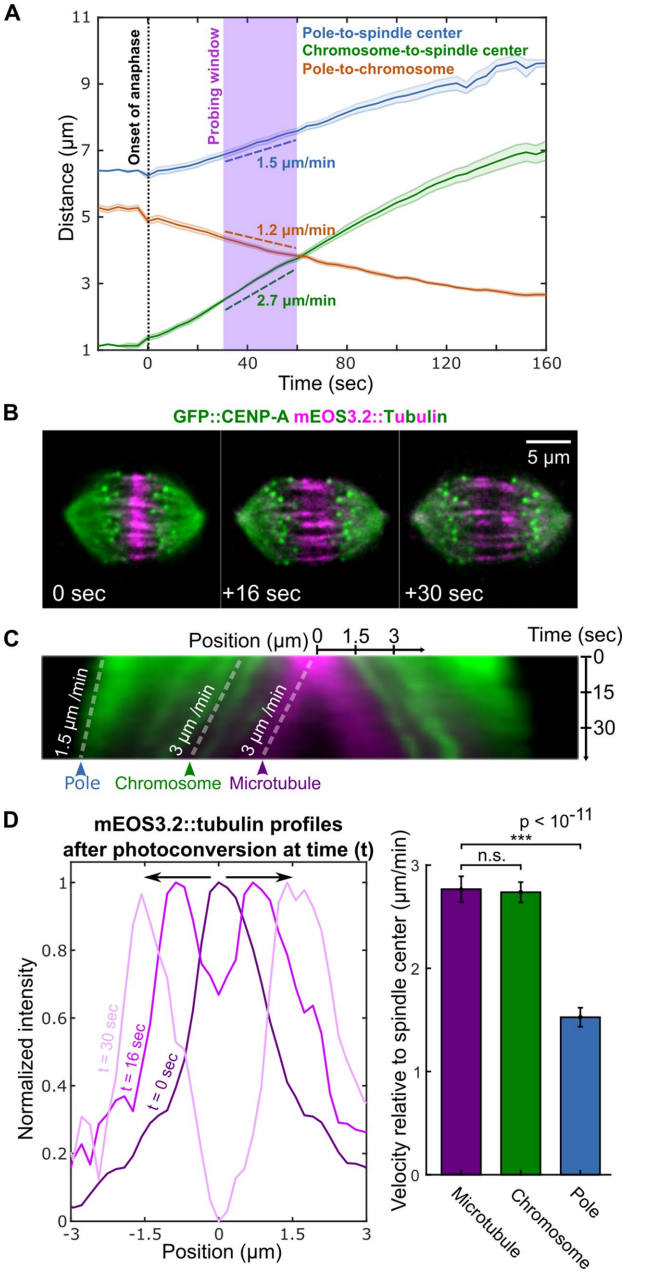

FIGURE 2: Central-spindle microtubules move apart at the same speed as chromosomes in human mitotic spindles. (A) Change of pole-to-spindle center (blue), chromosome-to-spindle center (green), and chromosome-to-pole (orange) distances during chromosome segregation. The slopes show the averaged velocity of the above three quantities during the probing window (purple), in which the experiments and observations were conducted. (B) Time-lapse images of GFP::CENP-A (green) and mEOS3.2::tubulin (green before photoconversion; magenta after photoconversion) human mitotic spindles with photoconverted microtubules between chromosomes. Time 0 is the onset of photoconversion. (C) A kymograph of the spindle shown in B, with white dashed lines illustrating that the photoconverted microtubules and chromosomes move apart at the same speed, and both are faster than poles. (D) Line profiles of photoconverted mEOS3.2-tubulin between chromosomes after photoconversion (left) from the kymograph in C, with arrows to indicate the split of the photoconverted region. Bar plot of velocities of microtubules (magenta), chromosomes (green), and spindle poles (blue) in human mitotic spindles 30–60 s after the onset of anaphase (right). Error bars are SEM (n.s., not significant).

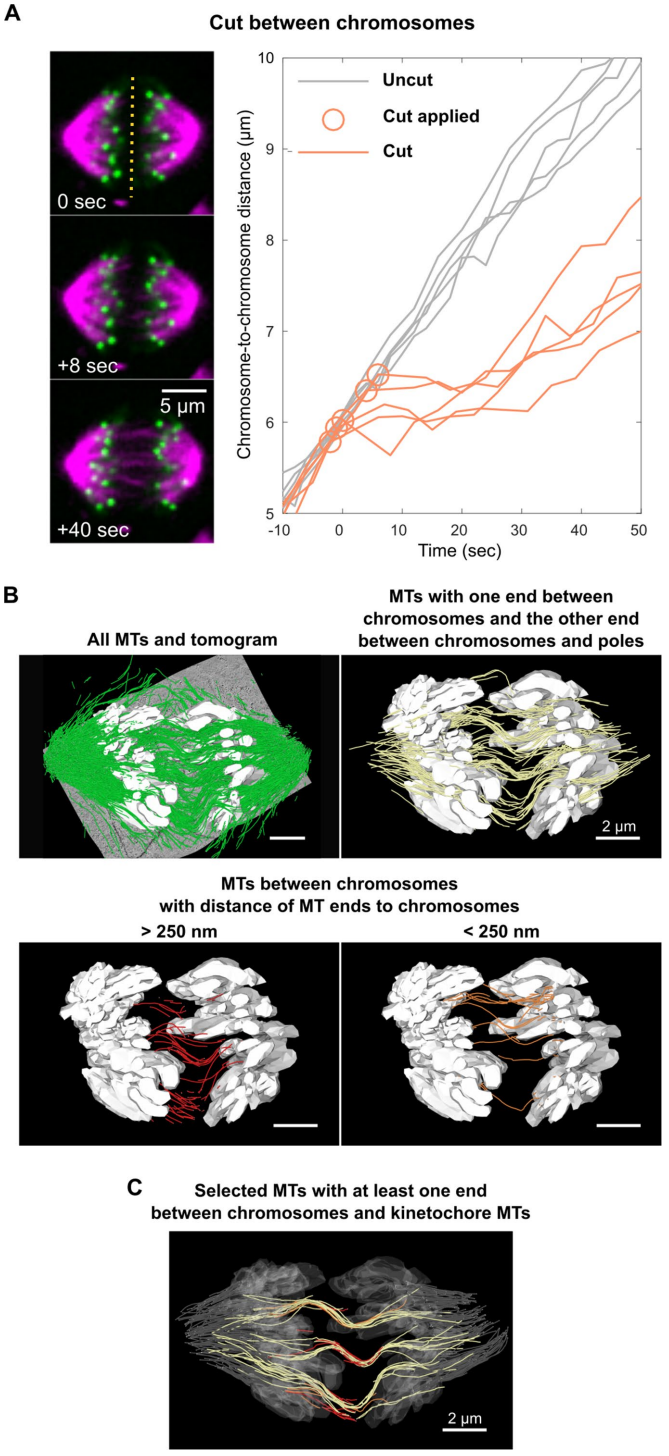

FIGURE 3: The functional and structural characterization of central-spindle microtubules in human mitotic spindles. (A) Time-lapse images of GFP::CENP-A (green) and mCherry::tubulin (magenta) human mitotic spindles with laser ablation of microtubules between chromosomes (left). Dotted lines indicate the timing and location of laser ablation. Curves of interchromosome distance vs. time with laser ablation of microtubules between chromosomes (orange) with uncut spindles (gray) for reference (right). (B) Electron tomographic reconstruction of microtubules in human mitotic spindles showing all microtubules (green, top left) overlaid on the tomogram. Some microtubules have both ends between chromosomes, with neither (red, bottom left) or either one (orange, bottom right) of their ends contacting chromosomes; other microtubules have only one end between chromosomes (yellow, top right). (C) Electron tomographic reconstruction of selective microtubule bundles consisting of the three classes of microtubules (red, orange, and yellow) in B, kinetochore microtubules (gray), and chromosomes (translucent).

microtubules and chromosomes move at the same speed in human mitotic anaphase spindles, even at times when anaphase A and anaphase B occur simultaneously, suggesting a coupling between them.

Laser-ablating central-spindle microtubules immediately stops anaphase chromosome motion in human mitotic spindles

We next sought to investigate to what extent central-spindle microtubules are coupled to chromosome motion in human mitotic spindles. We built a custom laser ablation system utilizing an ultrafast femtosecond laser, which enables subdiffraction-limited cuts (Vogel *et al.*, 2005) in nearly arbitrary three-dimensional patterns. These cuts are performed within a few seconds and generate minimal collateral damage outside of the ablated region (see *Materials and Methods*). We performed a rectangular plane-cut, 12 µm in length by 6 µm in depth, perpendicular to the spindle axis between separating chromosomes 30–60 s after the onset of anaphase (Figure 3A, left; Supplemental Movie S2). This ablation led to an immediate cessation of chromosome motion, reducing its speed to 0.1 ± 0.3 µm/min ($n = 6$; indistinguishable from 0, $p = 0.83$). When the motion of chromosomes stopped in response to disrupting the central-spindle, the chromosomes-to-pole distance continued to decrease at a speed of 0.7 ± 0.2 µm/min ($n = 14$), indistinguishable from the speed of 0.8 ± 0.2 µm/min ($n = 9$) in uncut spindles ($p = 0.71$) (Supplemental Figure S1). After ~20 s, chromosome segregation resumed with a speed similar to that of controls, presumably due to the microtubule regrowth, replacing the damaged population of microtubules (Figure 3A, right). In contrast, chromosome segregation continued (at a reduced rate) after ablating a region between chromosomes and poles (Supplemental Figure S2), while ablating an area in the cytoplasm did not impact the rate of chromosome motion (Supplemental Figure S3), which strongly argues that the observed pause in chromosome segregation after ablating the central-spindle is not a generic stress response to cellular damage from the laser. The finding that damaging the central-spindle in anaphase leads to the immediate cessation of chromosome motion further argues that central-spindle microtubules are strongly coupled to chromosome motion, even at times when anaphase A and anaphase B occur simultaneously.

Electron tomography reveals the presence of interchromosomal microtubules in human mitotic spindles

To further investigate how the central-spindle microtubules are coupled with chromosomes, we next studied the structure of human mitotic spindles in anaphase using large-scale electron tomographic reconstructions (Figure 3B, green). This work revealed the presence of interchromosomal microtubules: some of which had two free ends between chromosomes (Figure 3B, red), others of which had one end near the center of the spindle, with the other end contacting chromosomes (Figure 3B, orange). Other microtubules extended from the interchromosomal region, passed chromosomes, reaching a micron or so beyond them (Figure 3B, yellow). We found no microtubules, which extended all the way from the pole to the region between chromosomes, and no microtubules, which passed across the entire interchromosomal region,

directly bridging microtubules between the two poles. The three classes of microtubules we observed are often tightly associated into bundles, which appear to connect interchromosomal microtubules to kinetochore microtubules, near chromosomes (Figure 3C). The microtubules from a single interchromosomal bundle spread out and associate with multiple kinetochore fibers, showing that there is not a simple one-to-one correspondence between interchromosomal bundles and kinetochore fibers. This structure illustrates how interchromosomal microtubules in the central-spindle region may cross-link to kinetochore microtubules, which thus would couple the motion of central-spindle microtubules to the motion of chromosomes. This structure of central-spindle microtubules is reminiscent of what was previously seen in PtK1 cells (Mastronarde *et al.*, 1993).

Central-spindle microtubules slide apart at the speed of chromosome motion in *C. elegans* anaphase mitotic spindles

Having characterized dynamics, function, and structure of central-spindle microtubules in human mitotic spindles, we next explored whether central-spindle microtubules in other spindles have similar behavior and organization. We first set out to measure the relative motion of central-spindle microtubules and chromosomes in anaphase *C. elegans* mitotic spindles expressing GFP::tubulin and mCherry::histone. We were unable to reliably photobleach central-spindle microtubules in *C. elegans* mitotic spindles due to the rapid oscillations of these spindles in anaphase (Supplemental Movie S3). To better maintain the spindle in the focal plane, we knocked down GPR-1/2 using RNA interference (RNAi), which greatly reduces the cortically pulling forces (Supplemental Movie S4) (Grill *et al.*, 2003; Srinivasan *et al.*, 2003; Park and Rose, 2008). To understand the effect of *gpr-1/2(RNAi)* on chromosome segregation, we acquired time-lapse images of spindles for the first 3 min of anaphase in the first mitotic division of wild-type and *gpr-1/2(RNAi) C. elegans* embryos (Figure 4A; Supplemental Movies S3 and S4) and averaged the traces of pole motion, chromosome motion, and chromosome-to-pole motion (Figure 4B). In the wild-type embryos, the chromosome-to-pole distance stayed almost constant during this time (Figure 4B, top, orange) (Oegema *et al.*, 2001), that is, the mean speed of chromosomes, 1.1 ± 0.02 μm/min, was indistinguishable from the mean speed of poles, 1.1 ± 0.05 μm/min (Figure 4C, top, $n = 5$, $p = 0.93$). In contrast, time-lapse microscopy of *gpr-1/2(RNAi)* embryos showed that while pole motion was significantly reduced, the speed and extent of chromosome motion remained very similar to that in controls (compare Figure 4A, top and bottom; Supplemental Movies S3 and S4). We averaged the traces of pole motion, chromosome motion, and chromosome-to-pole motion and found that the

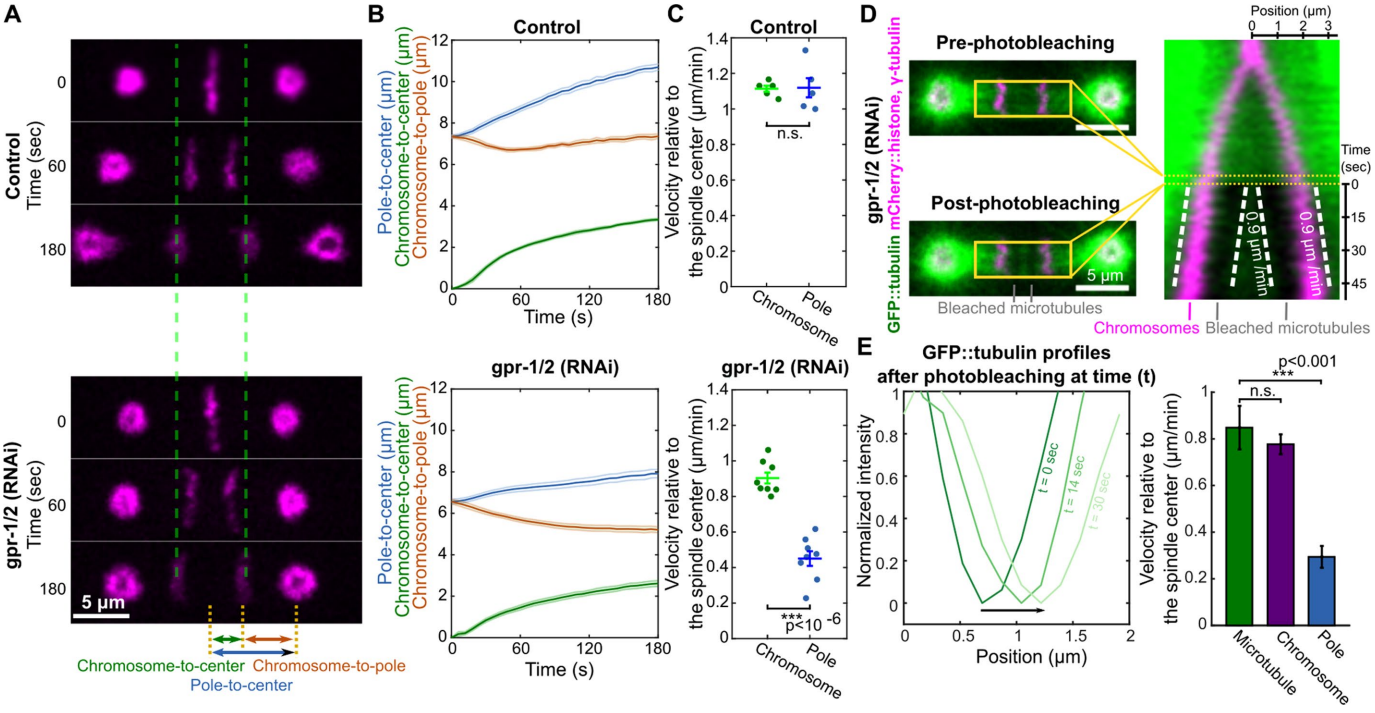

FIGURE 4: Central-spindle microtubules move apart at the same speed as chromosomes in *C. elegans* mitotic spindles. (A) Time-lapse images of mCherry::histone and mCherry::γ-tubulins (magenta) in control (top) and *gpr-1/2 (RNAi)* (bottom) spindles. Time 0 is the onset of anaphase. (B) Averaged pole-to-spindle center distance (blue), chromosome-to-spindle center distance (green), and chromosome-to-pole distance (orange) in control (top, $n = 5$) and *gpr-1/2 (RNAi)* (bottom, $n = 8$) embryos. (C) Scatter plots of velocities of chromosomes (green) and spindle poles (blue) in control (top, $n = 5$) and *gpr-1/2 (RNAi)* (bottom, $n = 8$) embryos during the first 3 min of anaphase. Error bars are SEM (n.s., not significant). (D) Images of a GFP::tubulin (green), mCherry::histone and mCherry::γ-tubulin (magenta) spindle before and after photobleaching, indicting the location of photobleached regions (left). A kymograph from the indicated region, with white dashed lines illustrating that the bleached regions and chromosomes move apart at the same speed (right); time 0 is the onset of photobleaching. (E) Line profiles of GFP-tubulins (left) over the region corresponding to the kymograph in (D), with an arrow to indicate the shift of the photobleached region. Bar plot of velocities of microtubules (green), chromosomes (purple), and spindle poles (blue) in *gpr-1/2 (RNAi)* embryos 40–60 s after the onset of anaphase (right). Error bars are SEM (n.s., not significant).

distance between chromosomes and poles continuously decreased over the course of anaphase (Figure 4B, bottom, orange), as the mean speed of poles, 0.45 ± 0.04 μm/min was significantly less than the mean speed of chromosomes, 0.90 ± 0.03 μm/min (Figure 4C, bottom, $n = 8$, $p < 10^{-6}$). Consistent with previous results (Nahaboo *et al.*, 2015), this experiment demonstrates that cortically pulling forces are not required for chromosome segregation in *C. elegans* mitosis. Since GPR-1/2 knockdown greatly reduced spindle movement and only had a minor impact on chromosome motion, we used this RNAi condition to investigate the relative motion of chromosomes and central-spindle microtubules.

We conducted photobleaching experiments in *gpr-1/2(RNAi)* embryos 40–60 s after the onset of anaphase, when the chromosome-to-pole speed was 0.5 ± 0.07 μm/min ($n = 7$) and the pole-to-spindle center speed was 0.3 ± 0.05 μm/min ($n = 7$). Thus, at this time, the chromosome-to-pole distance shrank at a faster rate than the poles separate (i.e., anaphase A and anaphase B were both underway at this time). We photobleached GFP-labeled tubulin to create two parallel fiducial marks on microtubules near the spindle center (Figure 4D, left). Kymographs showed that these fiducial marks moved apart at a speed similar to the speed of chromosomes separation (Figure 4D, right). The movement of the photobleached marks demonstrates that microtubules between chromosomes slide apart in anaphase. To further quantify this motion, we took line profiles of the bleached region (Figure 4E), tracked their motion and the motion of chromosomes (see *Materials and Methods*), and found that the central-spindle microtubules move at a speed of 0.8 ± 0.09 μm/min ($n = 7$), which is indistinguishable from the speed of chromosome movement (0.8 ± 0.04 μm/min, $n = 7$, $p = 0.53$) and substantially greater than the speed of pole movement (0.3 ± 0.05 μm/min, $n = 7$, $p < 0.001$). Therefore, our results reveal that central-spindle microtubules slide apart at the same speed as chromosomes, even at times when anaphase A and anaphase B occur simultaneously. Similar to the results in the human mitotic spindles, these results argue for a coupling between the central-spindle microtubules and chromosomes in *C. elegans* mitotic spindles.

Laser-ablating central-spindle microtubules immediately stops anaphase chromosome motion in *C. elegans* mitotic spindles

We next sought to investigate the coupling between the central-spindle microtubules and the chromosomes in *C. elegans* mitotic spindles using our custom laser ablation system. We first cut a rectangular plane, 4 μm in length by 6 μm in depth, perpendicular to the spindle axis halfway-through between separating chromosomes in *gpr-1/2(RNAi)* embryos (Figure 5A; Supplemental Movie S5). Cuts were performed 30–60 s after the onset of anaphase when chromosomes and poles move away from the spindle center at a speed of 1.2 ± 0.1 and 0.5 ± 0.1 μm/min, respectively, so that chromosomes move toward poles at a speed of 0.7 ± 0.1 μm/min. Thus, at this time, the chromosome-to-pole distance shrinks at a faster rate than the poles separate (i.e., anaphase A and anaphase B were both underway at this time). The ablation led to an immediate cessation of chromosome motion, reducing its speed to 0.1 ± 0.2 μm/min ($n = 7$; indistinguishable from 0, $p = 0.73$). After approximately ~20 s, chromosome segregation resumed with a speed similar to that of the uncut controls, presumably due to microtubule regrowth and replacement of the damaged microtubule population (Figure 5A, right). Thus, ablating microtubules between chromosomes completely stopped chromosome motion, while, at the time of these cuts, chromosome-to-pole distance was decreasing and spindle poles were separating. The result further argues that the central-spindle microtubules are strongly coupled to chromosome motion in *gpr-1/2(RNAi) C. elegans* embryos.

This strong coupling in the embryos with GPR-1/2 depleted might be due to an activation of compensatory processes not present in wild-type embryos. To test the coupling between central-spindle microtubules and chromosomes in the wild-type embryos, we ablated two rectangular regions, 8 μm in length by 6 μm in depth, between chromosomes and spindle poles on both sides of the spindle (Figure 5B, left) while the sister chromosomes were moving apart. After the cuts, the spindle poles detached from the central body of the spindle (Figure 5B, middle, green) and rapidly moved apart at a speed of 60.8 ± 2.2 μm/min ($n = 13$). In the subsequent ~15 s the poles underwent irregular movements while the central body of the spindle showed no correlated displacement or rotation, further arguing that the cut disconnected the central body of the spindle from the poles (Supplemental Movie S6). Chromosome segregation continued after the cuts (Figure 5B, middle, magenta). The cuts did not pause chromosome motion, but reduced their speed from 9.2 ± 0.3 μm/min ($n = 7$) in controls to 5.2 ± 0.1 μm/min ($n = 13$, $p < 10^{-10}$) (Figure 5B, right). Thus, while previous work showed that *C. elegans* mitotic spindles can segregate chromosomes if the poles are destroyed before the onset of anaphase (Nahaboo *et al.*, 2015), our new results demonstrate that chromosomes can continue segregating even immediately after severing the connection between chromosomes and poles in anaphase. The continued motion of chromosomes after sudden detachment from both spindle poles argues that, even in wild-type *C. elegans* mitotic embryos, the central-spindle microtubules are coupled to chromosomes in a manner that is not entirely dependent on connections through spindle poles.

The anaphase *C. elegans* mitotic spindle contains interchromosomal microtubules

To further investigate how the central-spindle microtubules couple to chromosomes, we performed serial-section electron tomography to reconstruct the *C. elegans* anaphase mitotic spindles (Figure 5C, left). Our reconstructions revealed the presence of interchromosomal microtubules: some of which had two free ends between chromosomes (Figure 5C, red), others of which had one end near the center of the spindle, with the other end contacting chromosomes (Figure 5C, orange). In addition, there are also microtubules with one end extending from the interchromosomal region passing around chromosomes to contact kinetochore microtubules (Figure 5C, yellow). Again, we also found no microtubules, which extended all the way from the pole to the region between chromosomes, and no microtubules, which passed across the entire interchromosomal region directly bridging microtubules between the two poles. Therefore, electron tomography demonstrates that interchromosomal microtubules also exist in anaphase *C. elegans* mitotic spindles, similar to those in human anaphase spindles. This structure suggests that either the coupling from central-spindle microtubules to chromosomes could be through direct contacts at the inner surface of chromosomes (Figure 5C, orange microtubules) or, alternatively, the connection to chromosomes could be indirect, by microtubules with one end extending from the interchromosomal region passing around chromosomes to contact kinetochore microtubules (Figure 5C, yellow). The lack of microtubules connecting the central-spindle region directly to the poles may explain the continued motion of chromosomes immediately after severing the connections between poles and chromosomes in anaphase.

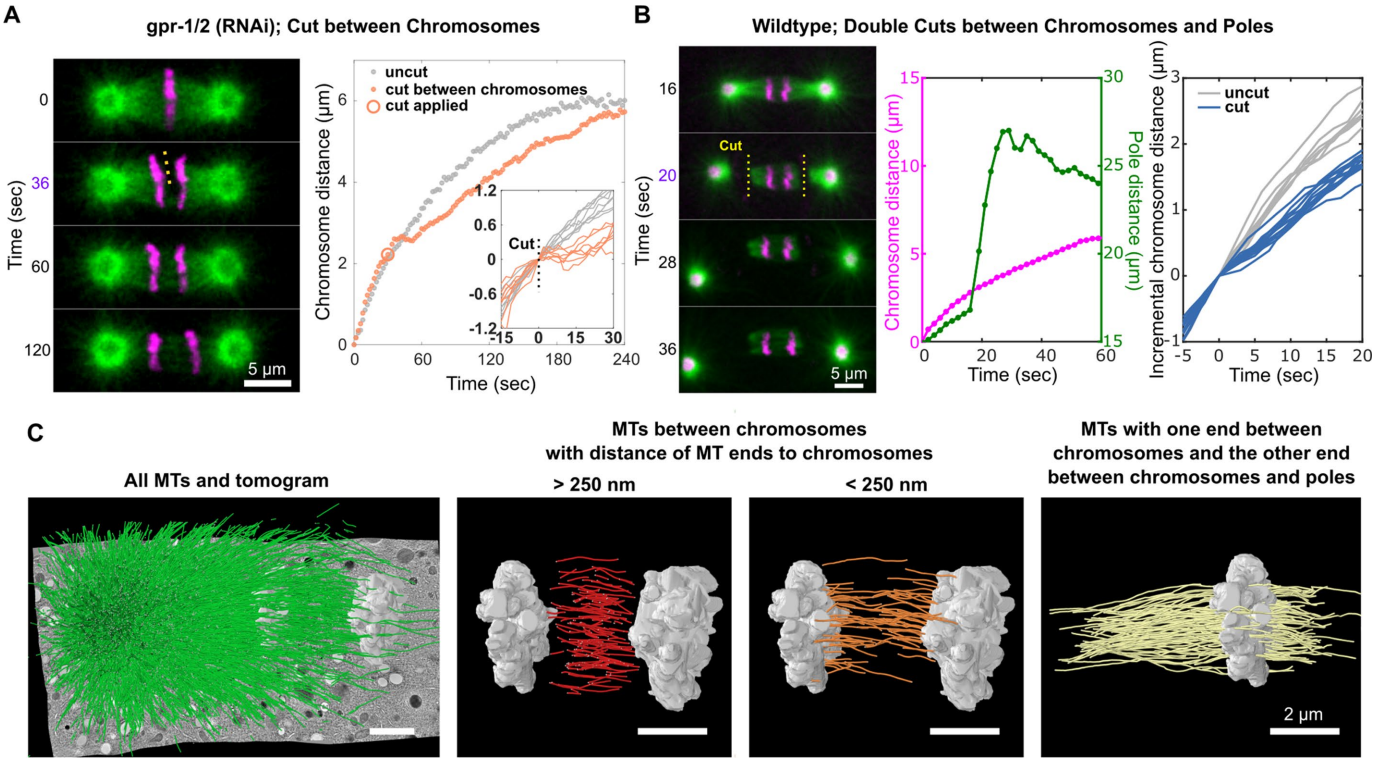

FIGURE 5: Functional and structural characterization of central-spindle microtubules in *C. elegans* mitotic spindles. (A) Time-lapse images of GFP::tubulin (green) and mCherry::histone (magenta) in *gpr-1/2 (RNAi) C. elegans* spindles (left) when microtubules are cut between chromosomes. Time 0 is the onset of anaphase. Dotted lines indicate the timing and location of laser ablation. Corresponding plots (right) of chromosome distance as a function of time, with an uncut spindle (gray) for reference. Example plots (right, inserts) of the change in chromosome distance after the cut from multiple spindles aligned relative to the timing of the cut, with uncut spindles (gray) for reference. (B) Time-lapse images of GFP::tubulin (green) and mCherry::histone, γ-tubulin (magenta) in wild-type *C. elegans* spindles when microtubules are cut between chromosomes and poles on both sides of the spindle (left). Time 0 is the onset of anaphase. Yellow dotted lines indicate the timing and location of laser ablation. Corresponding traces of chromosome-to-chromosome distance and pole-to-pole distance to the time-lapse image as a function of time (middle). Example plots of the change in chromosome distance after the cut from multiple spindles aligned relative to the timing of the cut, with uncut spindles (gray) for reference (right). (C) Electron tomographic reconstruction showing all traced microtubules (green) overlaid on a tomogram; some microtubules have both ends between chromosomes, with neither end (red) or either one (orange) contacting chromosomes; other microtubules have only one end between chromosomes (yellow, all such microtubules in a half-spindle).

Electron tomography confirms the presence of interchromosomal microtubules in *C. elegans* female meiosis

Having characterized the dynamics, function, and structure of central-spindle microtubules in human and *C. elegans* mitotic spindles, we next sought to apply the same approach to study a spindle with very different morphology and dynamics: acentrosomal *C. elegans* female meiotic spindles. We first generated electron tomographic reconstructions of all microtubules in *C. elegans* female meiotic spindles at various stages of anaphase (Figure 6A, left). Nearly all microtubules in the spindle lie between chromosomes at these stages of anaphase (Figure 6A, left). The organization of interchromosomal microtubules in *C. elegans* female meiotic spindles is highly reminiscent of those found in *C. elegans* mitotic spindles: some microtubules have both their ends between the chromosomes, without touching the chromosomes (Figure 6A, center), while some microtubules make end-on contact with chromosomes, with their other end terminating between the chromosomes (Figure 6A, right). Our observation of numerous interchromosomal microtubules in anaphase of *C. elegans* female meiotic spindles is consistent with previous partial electron tomography reconstructions (Laband *et al.*, 2017).

Laser-ablating central-spindle microtubules immediately stops anaphase chromosome motion in *C. elegans* meiotic spindles

To test the coupling of these interchromosomal microtubules to chromosomes, we used laser ablation to cut them during anaphase (Figure 6B; Supplemental Movie S7). We found that, as in mitotic spindles, this damage caused an immediate cessation of chromosome motion, with their speed reducing to 0.01 ± 0.01 µm/min (n = 6; indistinguishable from 0, p = 0.36) from a speed of 0.7 ± 0.1 µm/min (n = 5) in controls (Figure 6C). Similar to mitotic spindles, chromosome motion resumed at a speed similar to that of controls after ~20 s, presumably due to the spontaneous repair of the damaged population of microtubules. Thus, this result demonstrates that interchromosomal microtubules are strongly coupled to chromosomes in *C. elegans* female meiotic spindles at the stages we studied. A previous laser ablation study also found that cutting interchromosomal microtubules halted chromosome motion in *C. elegans* meiotic spindles (Laband *et al.*, 2017), although in that study, severed spindles never recovered, likely due to severe collateral damage caused by using a UV laser for ablation.

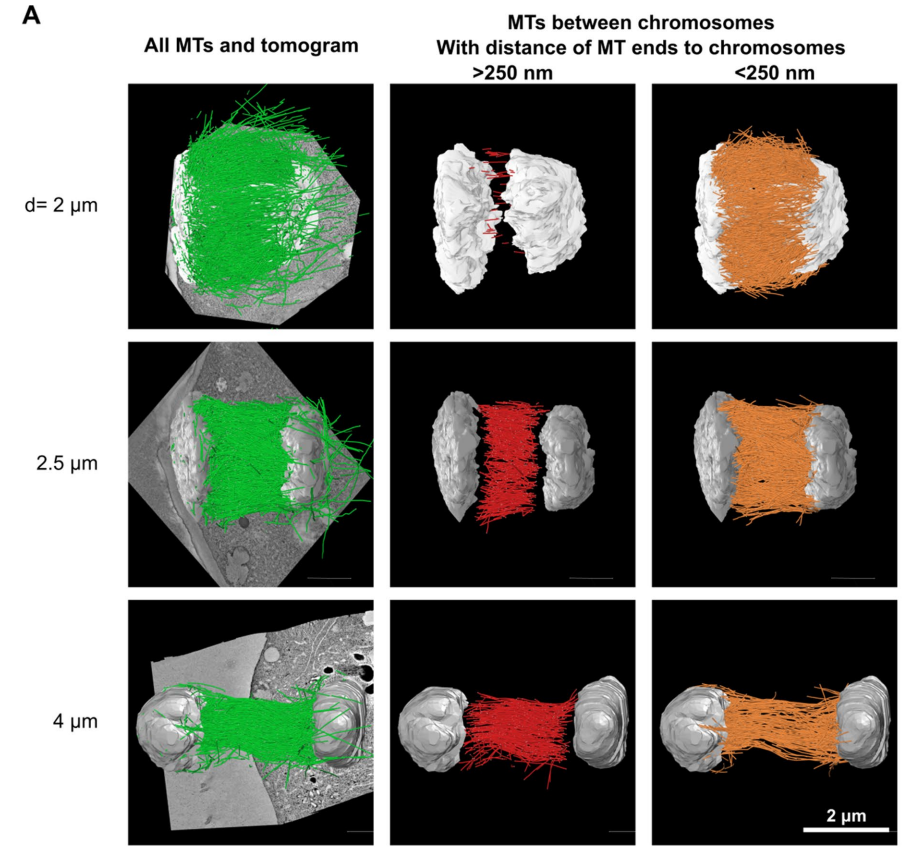

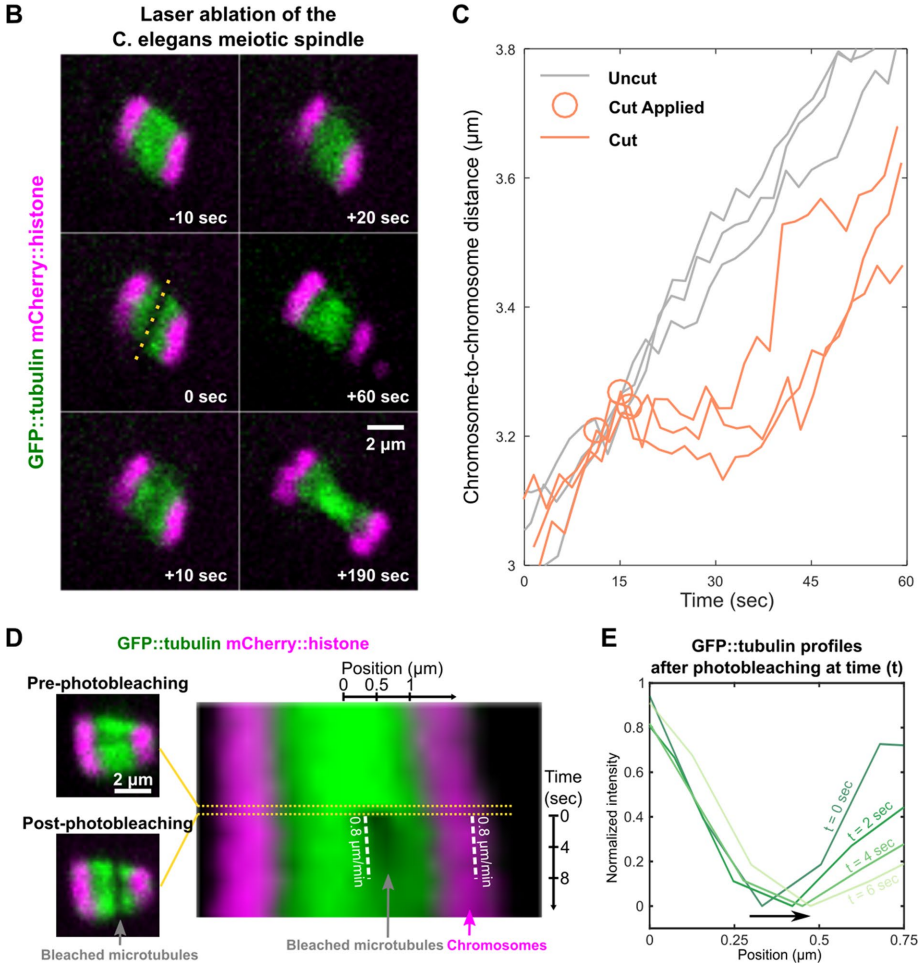

Interchromosomal microtubules slide apart at the speed of chromosome motion in *C. elegans* female meiotic spindles

We next investigated the relative motion of interchromosomal microtubules and chromosomes in *C. elegans* female meiotic spindles (Figure 1). We photobleached GFP-labeled tubulin to create a fiducial mark on interchromosomal microtubules adjacent to a set of sister chromosomes during anaphase and found that they moved at a similar speed as chromosomes moved (Figure 6D). To better quantify this motion, we made line profiles of the photobleached regions and tracked their motion, along with the motion of chromosomes (Figure 6E) (see *Materials and Methods*). Averaging measurements over multiple spindles gave a mean speed of microtubule sliding away from the spindle center of 0.5 ± 0.2 µm/min ($n = 6$), indistinguishable from the mean speed of chromosome movement, 0.3 ± 0.1 µm/min ($n = 6$, $p = 0.3$). These results further argue that central-spindle microtubules are strongly coupled to anaphase chromosomes in *C. elegans* female meiotic spindles.

FIGURE 6: Functional, structural, and dynamical characterization of interchromosomal microtubules in *C. elegans* female meiotic spindles. (A) Electron tomographic reconstructions of microtubules in *C. elegans* meiotic spindles with interchromosomal distances (d) of 2 µm (top row), 2.5 µm (middle row), and 4 µm (bottom row), showing all microtubules (green) overlaid on tomograms. Some microtubules have both ends between chromosomes, with neither (red) or either one (orange) of their ends contacting chromosomes. (B) Time-lapse images of a GFP::tubulin (green) and mCherry::histone (magenta) *C. elegans* meiotic spindle, with the dotted line indicating the timing and location of laser ablation. (C) Interchromosomal distance vs. time for spindles cut between chromosomes (orange), with uncut spindles (gray) for reference. (D) Images of a GFP::tubulin (green) and mCherry::γ-tubulin (magenta) spindle before and after photonbleaching (left), showing the position of the photobleached region (left). A kymograph of a spindle, with white dashed lines illustrating that the bleached regions and chromosomes move apart at the same speed; time 0 is the onset of photobleaching (right). (E) Line profiles of GFP-tubulin over the region corresponding to the kymograph in D, with an arrow to indicate the shift of the bleached center.

DISCUSSION

We used optical microscopy, laser ablation, and electron tomography to characterize central-spindle microtubules in anaphase in human mitotic spindles and *C. elegans* mitotic and female meiotic spindles. We found that central-spindle microtubules slide apart at the same speed as chromosomes, even at times when anaphase A and anaphase B occur simultaneously. Laser ablating central-spindle microtubules leads to an immediate cessation of chromosome motion, even at times when anaphase A and anaphase B occur simultaneously. These results argue that central-spindle microtubules are tightly coupled to chromosomes in anaphase. Because of technical limitations, our most detailed characterization of *C. elegans* mitotic spindles were performed when pulling forces were inhibited by *gpr-1/2(RNAi)*, a perturbation that only minimally impacted chromosome motion (while greatly reducing pole oscillations and movements). Our laser ablation experiments demonstrate that chromosomes continue to separate even immediately after severing the connection between chromosomes and poles, suggesting that a tight coupling between central-spindle microtubules and chromosomes is also present in wild-type *C. elegans* mitotic spindles.

It has previously been reported that damaging the central-spindle results in faster chromosome segregation in some systems, including in *C. elegans* mitotic spindles and in some vertebrate spindles (Aist and Berns, 1981; Aist and Bayles, 1991; Aist *et al.*, 1993; Sakai *et al.*, 1982; Bayles *et al.*, 1993; Grill *et al.*, 2001). In other systems, it has been reported that damaging the central-spindle impairs anaphase chromosome motion, including in human tissue culture cells and *C. elegans* meiotic spindles (Hiramoto and Nakano, 1988; Khodjakov *et al.*, 2004; Laband *et al.*, 2017; Vukusic *et al.*, 2017). It is possible that the central-spindle was only partially damaged in some of the previous studies that observed impaired, but continued, motion of chromosomes, and more complete damage might have halted chromosomes. Our interpretation of these diverse results is that the extent of chromosome motion after damaging the central-spindle is determined by the extent of the external pulling forces from outside of the spindle in different organisms (irrespective of whether those external pulling forces drive chromosome motion in undamaged spindles). We believe that the three types of wild-type spindles studied in our article are normally subject to different strengths of pulling forces, and thus, consistent with previous literature, respond differently to central-spindle damage. However, our results argue that central-spindle microtubules are strongly coupled to chromosomes in both anaphase A and anaphase B in all of these spindles.

To gain further insight into the manner by which central-spindle microtubules are coupled to chromosomes in anaphase, we also performed large-scale electron tomography reconstructions of these microtubules in human mitotic spindles and in *C. elegans* mitotic and female meiotic spindles (Supplemental Table S1). We found that all of these spindles contained microtubules with both ends between segregating chromosomes, some of which appeared to directly contact chromosomes. Human and *C. elegans* mitotic spindles also both contained microtubules with one end extending from the interchromosomal to contact kinetochore microtubules. In all the spindles we studied, we found no microtubules that extended all the way from the pole to the region between chromosomes and no microtubules that passed across the entire interchromosomal region, directly bridging kinetochore-microtubules from the opposite two poles. Thus, our data argue that central-spindle microtubules could be connected directly to chromosomes, or the coupling could be indirect through their mutual connection to kinetochore microtubules (or both). It is an exciting challenge for future research to disentangle these possibilities.

MATERIALS AND METHODS

C. elegans strains

Strain SA250 (tjIs54 [pie-1p::GFP::tbb-2 + pie-1p::2xmCherry::tbg-1 + unc-119(+)]; tjIs57 [pie-1p::mCherry::his-48 + unc-119(+)]) and a strain expressing GFP::tubulin and mCherry::histone (a gift from Marie Delattre's lab, Laboratoire de Biologie et Modélisation de la Cellule, Université de Lyon, France) were used for experiments of fluorescence imaging, laser ablation, and fluoresce recovery after photobleaching. Wild-type (N2) *C. elegans* embryos and oocytes were used for the preparation of electron tomography. All strains were cultured at 24°C and fed on OP50 bacteria on nematode growth medium plates.

Human cell lines and culture

Human bone osteosarcoma epithelial (U2OS) cells were engineered to stably express fluorescence-labeled proteins by retroviral transfections. Three stable fluorescence U2OS lines were used: one expresses GFP::CENP-A and mCherry::tubulin; another expresses GFP::centrin, GFP::CENP-A, and mCherry::tubulin; the other expresses GFP::CENP-A; and mEOS3.2::tubulin. U2OS cell lines were maintained in DMEM (Life Technologies), supplemented with 10% fetal bovine serum (Life Technologies) and 50 IU/ml penicillin and 50 µg/ml streptomycin (Life Technologies) at 37°C in a humidified atmosphere with 5% CO_2.

C. elegans imaging preparation and RNAi

For imaging of mitotic spindles, gravid *C. elegans* hermaphrodites were cut in half, and the released embryos were transferred onto a 4% agarose pad between a slide and a coverslip (Walston and Hardin, 2010). Meiotic spindles in oocytes were observed in uterus, as adult hermaphrodites were mounted between a coverslip and a thin 4% agarose pad on a slide. Polystyrene microspheres (microspheres 0.10 µm; Polysciences) in solution were added to help immobilize worms.

RNAi was carried out following the RNAi feeding protocol from the Ahringer lab (Kamath *et al.*, 2001). Plasmid pMD082 (a gift from the Marie Delattre lab) containing the sequence of *gpr-1/2* was cloned into the L4440 plasmid, which was transformed into HT115 bacteria. L2 hermaphrodites were transferred to *gpr-1/2 (RNAi)* plates and fed on the RNAi bacterial lawn for 36–48 h at 24°C.

Human cell imaging preparation

In preparation for imaging, cells were grown on a 25-mm-diameter, #1.5-thickness, round coverglass coated with poly-D-lysine (GG-25-1.5-pdl, neuVitro) to ~80–90% confluency. The cells were incubated in imaging media, which is FluoroBrite DMEM (Life Technologies) supplemented with 4 mM L-glutamine (Life Technologies) and 10 mM HEPES, for ~15–30 min before imaging. The coverglass was mounted on a custom-built temperature-controlled microscope chamber at 37°C, while covered with 1.5 ml of imaging media and 2 ml of white mineral oil. An objective heater (Bioptech) was used to maintain the objective at 37°C.

Sample preparation for electron tomography

Wild-type (N2) *C. elegans* embryos and oocytes collected in cellulose capillary tubes (Pelletier *et al.*, 2006; Redemann *et al.*, 2018) and HeLa Kyoto cells immobilized on sapphire disks (Guizetti *et al.*, 2011) were high-pressure frozen as described using either an EM PACT2+RTS or an EM ICE high-pressure freezer

(Leica Microsystems, Vienna, Austria) (Muller-Reichert *et al.*, 2007). Freeze substitution was performed over 2–3 d at –90°C in anhydrous acetone containing 1% OsO_4 and 0.1% uranyl acetate. Samples were embedded in Epon/Araldite and polymerized for 1–3 d at 60°C. Serial semithick sections (300 nm) were cut using an Ultracut UCT Microtome (Leica Microsystems, Vienna, Austria) collected on Formvar-coated copper slot grids and poststained with 2% uranyl acetate in 70% methanol followed by Reynold's lead citrate. For dual-axis electron tomography (Mastronarde, 1997), a series of tilted views were recorded using a TECNAI F30 transmission electron microscope (FEI Company, Eindhoven, The Netherlands) operated at 300 kV and equipped with a Gatan US1000 CCD camera (2k x 2k). Images were captured every 1.0° over a ±60° range. The IMOD software package (http://bio3d.colourado.edu/imod) was used for the calculation of electron tomograms (Kremer *et al.*, 1996). The Amira software package with an extension to the filament editor was used for the segmentation, automatic tracing, stitching, and 3D visualization of microtubules and for data analysis (Stalling *et al.*, 2005; Weber *et al.*, 2012, 2014).

Spinning disk confocal fluorescence imaging

Live imaging was performed using a spinning disk confocal microscope (Nikon Ti2000, Yokugawa CSU-X1) equipped with 488- and 561-nm diode lasers, an EMCCD camera (Hamamatsu), and a 60× water-immersion objective (CFI Plan Apo VC 60X WI, NA 1.2, Nikon). Acquisition parameters were controlled by a home-developed LabVIEW program (LabVIEW, National Instruments). For *C. elegans* mitotic and female meiotic spindles, images were acquired every 2 or 4 s with a single z-plane. For human mitotic spindles, images were acquired every 2 or 4 s with three z-sections every 1 µm, and the middle planes were presented.

Laser ablation

The laser ablation system was constructed on the above-mentioned spinning disk confocal microscope. Femtosecond-pulsed near-infrared lasers with either 80-MHz or 16-kHz repetition rate were adapted to perform laser ablation. Femtosecond pulses (80 MHz) with 0.3-nJ pulse energy and 800-nm center wavelength came directly from a Ti:sapphire pulsed laser (Mai-Tai; Spectra-Physics, Mountain View, CA). A 16-kHz femtosecond pulse train with ~6-nJ pulse energy was produced by selecting pulses from the above Ti:sapphire pulsed laser using a pulse picker (Eclipse Pulse Picker; KMLabs). The ablation laser was focused through the same objective for imaging, and laser ablation was performed by moving the sample on a piezostage (P-545 PInano XYZ; Physik Instrumente) in three dimensions controlled by a home-developed LabVIEW program (National Instruments). Scanning line cuts with z-steps were created by moving the stage perpendicular to the spindle long axis back and forth on the focal plane while lowering the stage in the z direction. The parameter for ablation in length by depth was 8 × 6 µm for *C. elegans* mitotic spindles, 12 × 6 µm for human mitotic spindles, and 6 × 2 µm for *C. elegans* meiotic spindles. The moving speed of the stage was 50 µm/s.

Photobleaching experiments

Photobleaching experiments used the same setup and software control as the laser ablation, except that a 80-MHz Ti:sapphire pulsed laser was used (800 nm wavelength, ~70 fs pulse width, ~0.1-nJ pulse energy; Mai-Tai; Spectra-Physics, Mountain View, CA). The parameter for photobleaching in length by depth was 7 × 6 µm in *C. elegans* mitotic spindles and 6 × 2 µm in C. elegans meiotic spindles. The moving speed of the stage was 50 µm/s.

Photoconversion experiments

Photoconversion experiments used the same setup and software control as the laser ablation, except that a 405-nm continuous-wave diode laser was used (Thorlabs). The parameter for photoconversion in length was 12 µm in human mitotic spindles. The moving speed of the stage was 50 µm/s.

Quantitative analysis in *C. elegans* mitotic spindles

Quantitative analysis of the chromosome distance with a subpixel resolution was achieved using a home-written MATLAB (MathWorks, Natick, MA) program. The center positions of two centrosomes in each frame of the time-lapsed images were either manually selected in spindles expressing GFP-labeled tubulin or automatically located in spindles expressing mCherry-labeled γ-tubulin based on a public MATLAB program for particle tracking (https://site.physics.georgetown.edu/matlab/index.html). The center positions of the two centrosomes in each frame determines the spindle long axis as well as the spindle length and were used to generate line scans of overlaid images of mCherry-labeled histones (corresponding to chromosomes). Averaged mCherry fluorescence intensities from histones along these line scans were extracted, and the fluorescence profile around histone-enriched regions were Gaussian-like shapes. A double-peak Gaussian function was used for fitting the line scans to locate the centers of two groups of histones, presumably reflecting the central positions of sister chromosomes. The distance of these two fitted center positions was defined as the chromosome-to-chromosome distance. A straight line was fitted to the change of chromosome distance versus time to extract the velocity of chromosome separation before and after laser ablation. In controls, the velocity was computed before and after the chromosome distance was 2.4 µm, the chromosome distance around which most laser-ablation experiments were performed.

Movement and recovery of photobleaching makers were also tracked using a program written in MATLAB. Line scans of GFP-labeled tubulin between chromosomes along the spindle axis were extracted over the course of anaphase. Each line scan at each time point can be divided into two halves by the middle plane of the spindle. The half of the line profile with the bleaching mark was normalized to the other half of the profile by a reflection of symmetry around the middle plane of the spindle. This profile normalization was used to remove spatial variations in the background fluorescence, a valid procedure assuming mirror symmetry of the spindle around its middle plane. A Gaussian function was used to fit the normalized profile to locate the center of the bleached mark, and thus the position of the bleached mark versus time was extracted. A straight line was fitted to the position of the bleached mark versus time to retrieve the velocity of the bleached mark.

Quantitative analysis in *C. elegans* meiotic spindles

Chromosome distance in *C. elegans* meiotic spindles was computed with a combination of Fiji (Schindelin *et al.*, 2012) and a MATLAB program. Time-lapse images of spindle expressing mCherry::histone (corresponding to chromosomes) were realigned in a routine for matching, rotation and translation using Rigid Body of Fiji's StackReg plug-in, so that the random displacement of the spindle due to the spontaneous motion of the worm was corrected. On the realigned time-lapse stack, a straight line passing through sister chromosomes was manually drawn in line with the spindle axis, and the kymograph of mCherry:histone intensities along this line was generated. On a MATLAB program, each line scan of mCherry:histone was fitted to a double-peak Gaussian function for

computing the center positions of sister chromosomes and thus the chromosome distance. A straight line was fitted to the data of chromosome distance versus time to extract the velocity of chromosome separation before and after laser ablation. In controls, separation velocity was computed before and after the chromosome distance was 3.3 µm, the chromosome distance around which most laser-ablation experiments were performed.

Movement of photobleaching makers was also tracked using a program written in MATLAB. Line scans of GFP-labeled tubulin between chromosomes along the spindle axis were extracted over the course of anaphase. A Gaussian function was used to fit the line-scanning profile to locate the center of the bleached mark, and thus the position of the bleached mark versus time was extracted. A straight line was fitted to the position of the bleached mark versus time to retrieve the velocity of the bleached mark.

Quantitative analysis in human mitotic spindles

Distance information of interest was extracted from spindles expressing GFP::CENP-A (corresponding to kinetochores) and GFP::centrins (corresponding to spindle poles) in time-lapse z-stacks based on the following steps. First, using approaches from a particle tracking algorithm (Pelletier *et al.*, 2009), a GUI MATLAB program was developed to retrieve the three-dimensional coordinates of the center positions of each kinetochores and the two poles. Next, a support vector machine algorithm was adapted to find the best plane to separate kinetochores of one half-spindle from those of the other half-spindle. This best plan is the one with the largest margin between two sides of kinetochores and corresponds to the middle plane of the spindle. A unit vector perpendicular to this plane was thus in line with the direction of spindle long axis. All positions of kinetochores and spindle poles in space were projected onto this unit vector and thus converted to one-dimensional information of projection lengths. Finally, chromosome-to-chromosome distance was computed as the length difference between the averaged projection lengths of kinetochores at one side of the half-spindle and those at the other side. Similarly, the chromosome-to-pole distance was computed as the length difference between averaged projection lengths of kinetochores and the projection length of the pole at the same side of the half-spindle. The above procedure was performed for each time point of a z-stack, so that the rotation and translation of spindles in space over the course of anaphase was corrected. A straight line was fitted to the data of chromosome-to-chromosome distance, and chromosome-to-pole distance versus time to compute the separation velocity of the chromosomes, and the velocity between chromosomes and poles before and after laser ablation, individually. In controls, the separation velocity of chromosomes was computed before and after the chromosome distance was at 6.1 µm.

Movement of photoconverted mEOS3.2-labeled microtubules were also tracked using a program written in MATLAB. Line scans of photoconverted tubulin between chromosomes along the spindle axis were extracted over the course of anaphase. A Gaussian function was used to fit the profile to locate the center of the photoconverted microtubules, and thus the position of the photoconverted microtubules versus time was extracted. A straight line was fitted to the position of the photoconverted microtubules versus time to retrieve the velocity of the photoconverted microtubules.

Statistical analysis

Statistics are presented as mean ± SEM, and *p* values were calculated by the "ttest2" function in MATLAB.

ACKNOWLEDGMENTS

We thank Marie Delattre for the *C. elegans* strain expressing GFP::tubulin and mCherry;tubulin and the bacteria containing the *gpr-1/2 (RNAi)* plasmid. We also thank Tobias Fürstenhaupt for technical assistance during acquisition of the tomographic data at the MPI-CBG (Max Planck Institute of Molecular Cell Biology and Genetics, Dresden). We thank Marie Delattre and John Calarco for discussions. The work was supported by the Human Frontier Science Program (RGP 7 0034/2010) to D.N., Marie Delattre, and T.M.R. The work of D.N. and C.-H.Y. was supported by the National Science Foundation grant DMR-0820484 and National Institutes of Health Grant 1R01GM104976-01. T.M.R. received funding from the German Research Foundation (DFG grant MU 1423/8-1 and 8-2) and from the Saxonian State Ministry for Science and the Arts (SMWK). S.R. was funded by the Frauenhabilitationsförderung of the Faculty of Medicine Carl Gustav Carus of the TU Dresden. R.K. received funding from the European Union's Horizon 2020 research and innovation programme under Marie Skłodowska-Curie grant agreement No 675737 (grant to T.M.R.).

REFERENCES

Aist JR, Bayles CJ (1991). Detection of spindle pushing forces in vivo during anaphase B in the fungus Nectria haematococca. Cell Motil Cytoskel 19, 18–24.

Aist JR, Berns MW (1981). Mechanics of chromosome separation during mitosis in Fusarium (Fungi imperfecti): new evidence from ultrastructural and laser microbeam experiments. J Cell Biol 91, 446–458.

Aist JR, Liang H, Berns MW (1993). Astral and spindle forces in PtK2 cells during anaphase B: a laser microbeam study. J Cell Sci 104(Pt 4), 1207–1216.

Asbury CL (2017). Anaphase A: disassembling microtubules move chromosomes toward spindle poles. Biology (Basel) 6, 15.

Bayles CJ, Aist JR, Berns MW (1993). The mechanics of anaphase-B in a basidiomycete as revealed by laser microbeam microsurgery. Exp Mycol 17, 191–199.

Brenner SL, Liaw LH, Berns MW (1980). Laser microirradiation of kinetochores in mitotic Ptk2 cells—chromatid separation and micronucleus formation. Cell Biophys 2, 139–152.

Brust-Mascher I, Civelekoglu-Scholey G, Kwon M, Mogilner A, Scholey JM (2004). Model for anaphase B: role of three mitotic motors in a switch from poleward flux to spindle elongation. Proc Natl Acad Sci USA 101, 15938–15943.

Cameron LA, Yang G, Cimini D, Canman JC, Kisurina-Evgenieva O, Khodjakov A, Danuser G, Salmon ED (2006). Kinesin 5-independent poleward flux of kinetochore microtubules in PtK1 cells. J Cell Biol 173, 173–179.

Chung SH, Clark DA, Gabel CV, Mazur E, Samuel AD (2006). The role of the AFD neuron in C. elegans thermotaxis analyzed using femtosecond laser ablation. BMC Neurosci 7, 30.

Ding R, McDonald KL, McIntosh JR (1993). Three-dimensional reconstruction and analysis of mitotic spindles from the yeast, Schizosaccharomyces pombe. J Cell Biol 120, 141–151.

Elting MW, Hueschen CL, Udy DB, Dumont S (2014). Force on spindle microtubule minus ends moves chromosomes. J Cell Biol 206, 245–256.

Ferenz NP, Ma N, Lee WL, Wadsworth P (2010). Imaging protein dynamics in live mitotic cells. Methods 51, 193–196.

Gattass RR, Mazur E (2008). Femtosecond laser micromachining in transparent materials. Nat Photonics 2, 219–225.

Grill SW, Gonczy P, Stelzer EH, Hyman AA (2001). Polarity controls forces governing asymmetric spindle positioning in the Caenorhabditis elegans embryo. Nature 409, 630–633.

Grill SW, Howard J, Schaffer E, Stelzer EH, Hyman AA (2003). The distribution of active force generators controls mitotic spindle position. Science 301, 518–521.

Guizetti J, Schermelleh L, Mantler J, Maar S, Poser I, Leonhardt H, Muller-Reichert T, Gerlich DW (2011). Cortical constriction during abscission involves helices of ESCRT-III-dependent filaments. Science 331, 1616–1620.

Hiramoto Y, Nakano Y (1988). Micromanipulation studies of the mitotic apparatus in sand dollar eggs. Cell Motil Cytoskeleton 10, 172–184.

Kamath RS, Martinez-Campos M, Zipperlen P, Fraser AG, Ahringer J (2001). Effectiveness of specific RNA-mediated interference through ingested double-stranded RNA in Caenorhabditis elegans. Genome Biol 2, RESEARCH0002.
Khodjakov A, Cole RW, Oakley BR, Rieder CL (2000). Centrosome-independent mitotic spindle formation in vertebrates. Curr Biol 10, 59–67.
Khodjakov A, Cole RW, Rieder CL (1997). A synergy of technologies: Combining laser microsurgery with green fluorescent protein tagging. Cell Motil Cytoskel 38, 311–317.
Khodjakov A, La Terra S, Chang F (2004). Laser microsurgery in fission yeast; role of the mitotic spindle midzone in anaphase B. Curr Biol 14, 1330–1340.
Konig K, Riemann I, Fischer P, Halbhuber KJ (1999). Intracellular nanosurgery with near infrared femtosecond laser pulses. Cell Mol Biol (Noisy-le-grand) 45, 195–201.
Kremer JR, Mastronarde DN, McIntosh JR (1996). Computer visualization of three-dimensional image data using IMOD. J Struct Biol 116, 71–76.
Kronebusch PJ, Borisy GG (1981). Anaphase pole movement after central spindle disruption in Ptk1 cells. J Cell Biol 91, A319–A319.
Laband K, Le Borgne R, Edwards F, Stefanutti M, Canman JC, Verbavatz JM, Dumont J (2017). Chromosome segregation occurs by microtubule pushing in oocytes. Nat Commun 8, 1499.
LaFountain JR Jr, Cohan CS, Siegel AJ, LaFountain DJ (2004). Direct visualization of microtubule flux during metaphase and anaphase in crane-fly spermatocytes. Mol Biol Cell 15, 5724–5732.
Ma N, Tulu US, Ferenz NP, Fagerstrom C, Wilde A, Wadsworth P (2010). Poleward transport of TPX2 in the mammalian mitotic spindle requires dynein, Eg5, and microtubule flux. Mol Biol Cell 21, 979–988.
Maiato H, Khodjakov A, Rieder CL (2005). Drosophila CLASP is required for the incorporation of microtubule subunits into fluxing kinetochore fibres. Nat Cell Biol 7, 42–47.
Mallavarapu A, Sawin K, Mitchison T (1999). A switch in microtubule dynamics at the onset of anaphase B in the mitotic spindle of Schizosaccharomyces pombe. Curr Biol 9, 1423–1426.
Mastronarde DN (1997). Dual-axis tomography: an approach with alignment methods that preserve resolution. J Struct Biol 120, 343–352.
Mastronarde DN, McDonald KL, Ding R, McIntosh JR (1993). Interpolar spindle microtubules in PTK cells. J Cell Biol 123, 1475–1489.
Masuda H, McDonald KL, Cande WZ (1988). The mechanism of anaphase spindle elongation: uncoupling of tubulin incorporation and microtubule sliding during in vitro spindle reactivation. J Cell Biol 107, 623–633.
McDonald KL, Edwards MK, Mcintosh JR (1979). Cross-sectional structure of the central mitotic spindle of Diatoma-vulgare—evidence for specific interactions between antiparallel microtubules. J Cell Biol 83, 443–461.
McDonald K, Pickett-Heaps JD, McIntosh JR, Tippit DH (1977). On the mechanism of anaphase spindle elongation in Diatoma vulgare. J Cell Biol 74, 377–388.
Mitchison TJ (1989). Polewards microtubule flux in the mitotic spindle: evidence from photoactivation of fluorescence. J Cell Biol 109, 637–652.
Mitchison TJ, Salmon ED (1992). Poleward kinetochore fiber movement occurs during both metaphase and anaphase-A in newt lung cell mitosis. J Cell Biol 119, 569–582.
Muller-Reichert T, Kiewisz R, Redemann S (2018). Mitotic spindles revisited—new insights from 3D electron microscopy. J Cell Sci 131.
Muller-Reichert T, Srayko M, Hyman A, O'Toole ET, McDonald K (2007). Correlative light and electron microscopy of early Caenorhabditis elegans embryos in mitosis. Methods Cell Biol 79, 101–119.
Nahaboo W, Zouak M, Askjaer P, Delattre M (2015). Chromatids segregate without centrosomes during Caenorhabditis elegans mitosis in a Ran- and CLASP-dependent manner. Mol Biol Cell 26, 2020–2029.
Nicklas RB (1989). The motor for poleward chromosome movement in anaphase is in or near the kinetochore. J Cell Biol 109, 2245–2255.
Oegema K, Desai A, Rybina S, Kirkham M, Hyman AA (2001). Functional analysis of kinetochore assembly in Caenorhabditis elegans. J Cell Biol 153, 1209–1226.
Park DH, Rose LS (2008). Dynamic localization of LIN-5 and GPR-1/2 to cortical force generation domains during spindle positioning. Dev Biol 315, 42–54.
Pelletier V, Gal N, Fournier P, Kilfoil ML (2009). Microrheology of microtubule solutions and actin-microtubule composite networks. Phys Rev Lett 102, 188303.
Pelletier L, O'Toole E, Schwager A, Hyman AA, Muller-Reichert T (2006). Centriole assembly in Caenorhabditis elegans. Nature 444, 619–623.
Pereira AJ, Aguiar P, Belsley M, Maiato H (2016). Inducible fluorescent speckle microscopy. J Cell Biol 212, 245–255.
Redemann S, Baumgart J, Lindow N, Shelley M, Nazockdast E, Kratz A, Prohaska S, Brugues J, Furthauer S, Muller-Reichert T (2017). C. elegans chromosomes connect to centrosomes by anchoring into the spindle network. Nat Commun 8, 15288.
Redemann S, Lantzsch I, Lindow N, Prohaska S, Srayko M, Muller-Reichert T (2018). A switch in microtubule orientation during C. elegans meiosis. Curr Biol 28, 2991–2997.e2992.
Sakai H, Mohri H, Borisy GG, Nippon Gatujutsu Shinkōkai., and Fujihara Kagaku Zaidan (1982). Biological Functions of Microtubules and Related Structures, New York: Academic Press.
Saxton WM, McIntosh JR (1987). Interzone microtubule behavior in late anaphase and telophase spindles. J Cell Biol 105, 875–886.
Schaffer CB, Brodeur A, Garcia JF, Mazur E (2001a). Micromachining bulk glass by use of femtosecond laser pulses with nanojoule energy. Optics Lett 26, 93–95.
Schaffer CB, Brodeur A, Mazur E (2001b). Laser-induced breakdown and damage in bulk transparent materials induced by tightly focused femtosecond laser pulses. Meas Sci Technol 12, 1784–1794.
Schindelin J, Arganda-Carreras I, Frise E, Kaynig V, Longair M, Pietzsch T, Preibisch S, Rueden C, Saalfeld S, Schmid B, *et al*. (2012). Fiji: an open-source platform for biological-image analysis. Nat Methods 9, 676–682.
Scholey JM, Civelekoglu-Scholey G, Brust-Mascher I (2016). Anaphase B. Biology (Basel) 5, 51.
Shen N, Datta D, Schaffer CB, LeDuc P, Ingber DE, Mazur E (2005). Ablation of cytoskeletal filaments and mitochondria in live cells using a femtosecond laser nanoscissor. Mech Chem Biosyst 2, 17–25.
Srinivasan DG, Fisk RM, Xu H, van den Heuvel S (2003). A complex of LIN-5 and GPR proteins regulates G protein signaling and spindle function in C. elegans. Genes Dev 17, 1225–1239.
Stalling D, Westerhoff M, Hege H-C (2005). Amira: a highly interactive system for visual data analysis. In: The Visualization Handbook, ed. CD Hansen and CR Johnson, New York: Elsevier, 749–767.
Supatto W, Debarre D, Moulia B, Brouzes E, Martin JL, Farge E, Beaurepaire E (2005). In vivo modulation of morphogenetic movements in Drosophila embryos with femtosecond laser pulses. Proc Natl Acad Sci USA 102, 1047–1052.
Vitek DN, Adams DE, Johnson A, Tsai PS, Backus S, Durfee CG, Kleinfeld D, Squier JA (2010). Temporally focused femtosecond laser pulses for low numerical aperture micromachining through optically transparent materials. Opt Express 18, 18086–18094.
Vogel A, Noack J, Huttman G, Paltauf G (2005). Mechanisms of femtosecond laser nanosurgery of cells and tissues. Appl Phys B-Lasers O 81, 1015–1047.
Vukusic K, Buda R, Bosilj A, Milas A, Pavin N, Tolic IM (2017). Microtubule sliding within the bridging fiber pushes kinetochore fibers apart to segregate chromosomes. Dev Cell 43, 11–23 e16.
Walston T, Hardin J (2010). An agar mount for observation of Caenorhabditis elegans embryos. Cold Spring Harb Protoc 2010, pdb.prot5540.
Watanabe W, Arakawa N, Matsunaga S, Higashi T, Fukui K, Isobe K, Itoh K (2004). Femtosecond laser disruption of subcellular organelles in a living cell. Opt Express 12, 4203–4213.
Weber B, Greenan G, Prohaska S, Baum D, Hege HC, Muller-Reichert T, Hyman AA, Verbavatz JM (2012). Automated tracing of microtubules in electron tomograms of plastic embedded samples of Caenorhabditis elegans embryos. J Struct Biol 178, 129–138.
Weber B, Tranfield EM, Hoog JL, Baum D, Antony C, Hyman T, Verbavatz JM, Prohaska S (2014). Automated stitching of microtubule centerlines across serial electron tomograms. PLoS One 9, e113222.
Winey M, Mamay CL, O'Toole ET, Mastronarde DN, Giddings TH Jr, McDonald KL, McIntosh JR (1995). Three-dimensional ultrastructural analysis of the Saccharomyces cerevisiae mitotic spindle. J Cell Biol 129, 1601–1615.
Winey M, Morgan GP, Straight PD, Giddings TH Jr, Mastronarde DN (2005). Three-dimensional ultrastructure of Saccharomyces cerevisiae meiotic spindles. Mol Biol Cell 16, 1178–1188.